

On the hysteretic behaviour of moist convection

By XIANG-YU HUANG, *Department of Meteorology,* University of Stockholm, Arrhenius Laboratory, S-106 91 Stockholm, Sweden*

(Manuscript received 16 February; in final form 15 August 1987)

ABSTRACT

A study of two-dimensional moist convection has been performed with a Boussinesq-approximated model, where the effect of moisture is only taken into account as a flow-dependent heating. We first investigate the characteristics of the model in a conditionally unstable stratification. Then by numerically integrating the model equations with a slowly varying static stability, we have also observed hysteretic behaviour as a quasi-equilibrium feature of the model. When the time scale of static stability changes is comparable to reality (12 h), the transition from a state of rest to finite amplitude convection is much quicker than the reversed process. This behaviour is directly related to the hysteresis phenomenon and gives a qualitative understanding of the dynamics of moist convection on a diurnal timescale.

1. Introduction

Hysteretic behaviour of moist convection may be observed by following the diurnal cumulus activity. After sunrise, the surface is heated and the vertical temperature gradient increases with time. When a critical value of the temperature gradient is reached, cumulus convection sets in and develops quickly. The temperature gradient decreases in the afternoon and so does the cumulus activity. However, cumulus convection may be maintained even when the temperature gradient is much smaller than that needed for the onset and the process for cumulus convection to be dissipated is slow compared to the onset process. This may be due to the fact that moist convection needs different static stabilities for its onset and its termination. The inertia effect may also contribute in further enhancing this phenomenon, i.e., after the stratification becomes unstable, some time is needed for the development of convection and vice versa.

In studies of dry convection, Krishnamurti (1968, 1975a, b) found vertical asymmetries in the horizontally averaged temperature field which gave rise to hysteretic behaviour. The physical origin of the vertically asymmetric

heating is the turbulent heat flux due to changing temperatures at the horizontal boundaries and the imposed vertical velocity fields. Oerlemans (1983) found hysteretic behaviour of a two-dimensional cloud model by showing the existence of multiple, statistically steady states for a reasonable range of moisture content and surface heat flux. In the atmosphere, each of these processes may be considered as an alternative cause for hysteretic behaviour. However, from an energetic point of view, condensation is the most important process in atmospheric convection and therefore must have a dominating influence on the hysteretic behaviour. Much insight into this problem can be gained from a low-order model for moist convection (Huang and Källén, 1986). In the low-order model, they found this type of behaviour which is due to a positive feedback between the condensational heating and convection. It is shown to be a robust model property within an atmospherically realistic range of parameter values.

In this study, we want to go one step further than the low-order model and include a large number of wave components in a spectral model. We first investigate the energy redistribution among the different scales of motion due to the nonlinear nature of condensational heating. Then studies of the impact of multi-wave dynamics

* Contribution no. 570.

upon the hysteretic behaviour are performed through numerical integrations. Different model behaviour during the onset and the termination of convection will be discussed as the time scale of a changing static stability is comparable with a diurnal time scale.

2. The model

As basic model equations, we choose the Boussinesq-approximated vorticity equation and the thermodynamic equation in a two-dimensional (y, z) plane (Huang and Källén, 1986):

$$\partial \nabla^2 \Psi / \partial t = -J(\Psi, \nabla^2 \Psi) + g\alpha \partial \Theta / \partial y + \nu \nabla^4 \Psi, \quad (2.1.a)$$

$$\partial \Theta / \partial t = -J(\Psi, \Theta) + S \partial \Psi / \partial y + \kappa \nabla^2 \Theta + Q, \quad (2.1.b)$$

where Ψ is the streamfunction in the (y, z) plane, Θ is the temperature deviation from a reference profile $T_0(z)$ and $J(A, B)$ denotes a Jacobian with respect to y and z . In the vorticity equation (2.1.a), g is the acceleration of gravity, α is the coefficient of thermal expansion and ν is the eddy diffusivity. In the thermodynamic equation (2.1.b), κ is the coefficient of thermal conductivity, Q is the condensational heating and S is the dry static stability which is defined as the difference between the basic temperature lapse rate Γ and the dry adiabatic lapse rate Γ_d . The Coriolis acceleration is omitted to make the situation as simple as possible. This is acceptable if we assume the background wind shear to be negligible and the time scale of convection to be small compared with the inertia time scale. When the numerical integration goes beyond a day, the omission of the Coriolis acceleration is a questionable assumption. However, when we explore the model sensitivity to the static stability, in particular to identify the critical values for the onset and the termination of moist convection, we will make long numerical integrations beyond a day. As we do not wish to model the atmosphere on these long time scales, but rather investigate the steady-state dynamics of the model, we feel justified in neglecting the Coriolis acceleration. Similarly, radiative processes are not explicitly included. Through the prescribed, background static stability, we have implicitly included radiative effects, but do not include the modified internal heating/cooling of the atmos-

phere which radiative processes give rise to in a cloudy atmosphere. This effect is most pronounced on a time scale of many days, but for the same reasons as stated above in connection with the Coriolis force, we neglect radiation even when our time integrations are extended to several days.

To simplify the problem, we assume that all condensed water rains out immediately so that condensation influences the model by latent heat release only above the height of the lifting condensation level (LCL) and in the region of ascending motion. The following expression is used for Q :

$$Q = \frac{L_v}{c_p} \frac{dq_s}{dt} \delta, \quad (2.2)$$

where q_s is the saturation specific humidity, c_p is the specific heat of air at constant pressure, L_v is the latent heat of condensation and δ is a Heaviside type of function

$$\delta = \begin{cases} 0 & \partial \Psi / \partial y \leq 0 \quad \text{or} \quad z \leq z_b, \\ 1 & \partial \Psi / \partial y > 0 \quad \text{and} \quad z > z_b, \end{cases} \quad (2.3)$$

where z_b is the height of the LCL. As z_b is determined only by the temperature and specific humidity at the lower boundary, it is kept constant as long as T and q_s at $z = 0$ are unchanged. By using the Clausius-Clapeyron equation, the thermodynamic equation (2.1.b) is modified to read

$$\partial \Theta / \partial t = -J(\Psi, \Theta) + S \partial \Psi / \partial y + \kappa \nabla^2 \Theta + (H^* \partial \Psi / \partial y - M \kappa \nabla^2 \Theta) \delta, \quad (2.1.b')$$

where H^* and M have the following definitions:

$$H^* = \Gamma_d - \Gamma_m, \quad (2.4)$$

$$M = \frac{\varepsilon L_v^2 q_s}{c_p R_d T^2 + \varepsilon L_v^2 q_s}. \quad (2.5)$$

In (2.4) and (2.5), Γ_m is the moist adiabatic lapse rate, R_v is the gas constant of water vapor and ε is the ratio between R_d , the gas constant of dry air, and R_v . While Γ and Γ_d are taken to be constant, H^* and M are assumed to be functions of z in the present study. More details of the derivations and discussions about H^* and M can be found in Huang and Källén (1986).

We nondimensionalize our variables as follows

$$\begin{aligned}
 y &= (d/\pi)y', \\
 z &= (d/\pi)z', \\
 t &= (d^2/\pi^2\kappa)t', \\
 \Psi &= \kappa\Psi', \\
 \Theta &= (\pi^3\nu\kappa/g\alpha d^3)\Theta',
 \end{aligned}
 \tag{2.6}$$

where d is the height of the model domain. Dropping the primes, the basic equations (2.1.a) and (2.1.b') may then be written:

$$\partial\nabla^2\Psi/\partial t = -J(\Psi, \nabla^2\Psi) + \sigma\partial\Theta/\partial y + \sigma\nabla^4\Psi,
 \tag{2.7.a}$$

$$\begin{aligned}
 \partial\Theta/\partial t &= -J(\Psi, \Theta) + R\partial\Psi/\partial y + \nabla^2\Theta \\
 &+ (H\partial\Psi/\partial y - M\nabla^2\Theta)\delta.
 \end{aligned}
 \tag{2.7.b}$$

In (2.7), the Prandtl number σ , the Rayleigh number R and the nondimensional heating coefficient $H(z)$ are defined as

$$\begin{aligned}
 \sigma &= \nu/\kappa, \\
 R &= g\alpha d^4 S/\pi^4\nu\kappa, \\
 H(z) &= g\alpha d^4 H^*/\pi^4\nu\kappa.
 \end{aligned}
 \tag{2.8}$$

The boundary conditions are as follows: horizontally, the motion is periodic; at the upper and lower boundaries, the temperature deviation is kept to zero and the streamfunction has free slip boundary conditions.

Due to the boundary conditions, we use trigonometric functions to expand Ψ and Θ . Furthermore, we assume that the convection cells extend from the bottom to the top of the model domain, i.e., only one component in the vertical is used for the streamfunction. In this study, we only consider the situation where the static stability is a constant in the vertical and the conditionally unstable layer therefore extends initially throughout the whole model domain. This is an important factor for the above assumption to be valid. If we want to include the development of a convective layer, more components in the vertical are necessary. This assumption has been tested in a numerical study with a grid point version of (2.1). This model can only be integrated for a short time, but the results clearly support the assumption of deep convective cells. In Section 3, a description of this experiment will be presented, where most of the convective cells extend vertically through the whole model domain, when the model stratifi-

cation is conditionally unstable. Similar results can also be found in Sheu et al. (1980).

To study scale selection in the model, we include a large number of horizontal components. The temperature deviation contains two more vertical components which have no horizontal variation to represent the modification of the mean stratification. The streamfunction Ψ and the temperature deviation Θ are written:

$$\begin{aligned}
 \Psi &= \sum_{n=1}^N \sqrt{2}(\Psi_{2n-1} \sin any \\
 &+ \Psi_{2n} \cos any) \sin z, \\
 \Theta &= \Theta_s \sin 2z + \Theta_h \sin z \\
 &+ \sum_{n=1}^N \sqrt{2}(\Theta_{2n} \sin any \\
 &+ \Theta_{2n-1} \cos any) \sin z,
 \end{aligned}
 \tag{2.9}$$

where n is the horizontal wave number, N is the maximum wave number, $a = 2d/L$ and L the length of the model domain.

The nonlinear nature of the condensational heating terms forces us to compute them in the physical domain; a transformation scheme is therefore implemented. The time integration is performed in the spectral domain and at each time step following the Fourier transformation of the physical variables, heating terms are computed in the physical domain and then transformed back to spectral space. Formally, we may write

$$\begin{aligned}
 C &= C_s \sin 2z + C_h \sin z + \sum_{n=1}^N 2(C_{2n} \sin any \\
 &+ C_{2n-1} \cos any) \sin z,
 \end{aligned}
 \tag{2.10}$$

where $C = [H(z)\partial\Psi/\partial y - M(z)\nabla^2\Theta]\delta$, which contains all condensational terms of the model. By inserting (2.9) and (2.10) into the basic equation (2.7) and using the orthogonality properties of the trigonometric functions we obtain the basic equations in spectral space:

$$\begin{aligned}
 \dot{\Psi}_m &= \sigma\{b(m)\Theta_m/[1+b(m)^2] - [1+b(m)^2]\Psi_m\}, \\
 \dot{\Theta}_m &= b(m)\Psi_m(R+\Theta_s) - [1+b(m)^2]\Theta_m + C_m, \\
 \dot{\Theta}_s &= -4\Theta_s - \sum_{k=1}^{2N} b(k)\Psi_k\Theta_k + C_s, \\
 \dot{\Theta}_h &= -\Theta_h + C_h,
 \end{aligned}
 \tag{2.11}$$

where, $m = 1, 2, \dots, 2N$ and

$$b(m) = \begin{cases} -ma/2 & m \text{ even} \\ (m+1)a/2 & m \text{ odd} \end{cases} \quad (2.12)$$

Finally, we give the definition of the mean kinetic energy:

$$E = -\left(\frac{a}{2\pi^2}\right) \frac{1}{2} \int_0^\pi \int_0^{2\pi/a} (\Psi \nabla^2 \Psi) dy dz = \sum_{n=1}^N E(n) \quad (2.13)$$

and its expression in spectral space

$$E(n) = \frac{1}{4} (1 + (an)^2)(\Psi_{2n-1}^2 + \Psi_{2n}^2). \quad (2.14)$$

3. Characteristics of moist convection

In order to get an idea of the characteristics of the spectral model, we first integrate (2.11) with a constant static stability which is conditionally unstable. A small random forcing is added on the right-hand side of every equation of (2.11) in the first 2 h so that any unstable component may grow. A leap-frog scheme is adopted for the time integration and the following time filtering scheme is used

$$\bar{F}(t) = F(t) + \gamma[F(t - \Delta t) + F(t + \Delta t) - 2F(t)], \quad (3.1)$$

where $F(t)$ can be any variable in (2.11) and γ is the filtering factor ($\gamma = 0.06$ in all integrations).

In Fig. 1, we show the time evolution of the mean kinetic energy, E . From a state of rest, E increases rapidly and then approaches an equilibrium state asymptotically. The growing stage is completed within about 2 h but the equilibrium state of the model has not been reached even after 8 h. This may be more clearly seen in Fig. 2, where the kinetic energy spectrum $E(n)$ as defined in (2.14) is shown at different time points. Only after about 10 h can we consider the kinetic energy spectrum to be in an equilibrium state. Furthermore, in order to show the slope of the spectrum, we show $E(n)$ at $t = 12.5$ h relative to an n^{-2} curve. As the model approaches equilibrium, more and more kinetic energy is concentrated in the largest scale of motion ($n = 1$). The final slope of $E(n)$ has nothing to do with two-dimensional turbulence theory, as the non-linearity due to vorticity advection is absent due

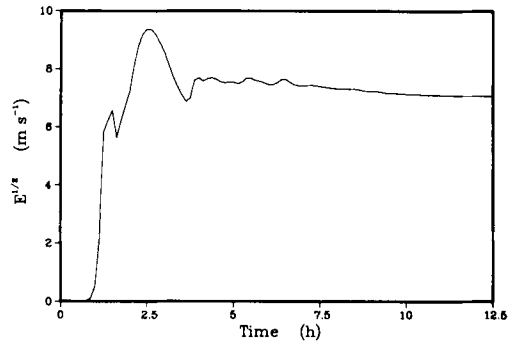


Fig. 1. Time evolution of the mean kinetic energy. The vertical axis is the square root of the mean kinetic energy ($E^{1/2}$) and the horizontal axis is the time (t). The parameters are:

- $\sigma = 1$
- $\alpha = 1/300 \text{ K}^{-1}$
- $T(0) = 287 \text{ K}$
- $S = -2.5 \text{ K km}^{-1}$
- $\nu = 100 \text{ m}^2 \text{ s}^{-1}$
- $a = 1/30$
- $\gamma = 0.06$
- $z_0 = 0 \text{ m}$
- $h = 3000 \text{ m}$
- $N = 50$

to the spectral truncation. The spectral characteristics are most easily explained through the motion field which has one narrow and intense updraft and very weak downward motion throughout the rest of the model domain. This may equally well be visualized from the time evolution of the motion field. As the convection continues, the ascending motion becomes more intense and narrower while the descending motion gets weaker and broader. This is mainly due to the conditionally unstable stratification. Without condensational heating, the flow organization is not very effective and a much longer time is needed for a slight modification in the energy spectrum to take place. As the model approaches its equilibrium state, only one updraft grid point is left, which is the winner after the competition among many updrafts generated by the random forcing at the beginning of the integration. To give a brief account of how convection cells develop and organize, we show the time evolution of the updraft pattern in Fig. 3. At first, a pattern of the updraft develops which is then kept for about 0.5 h. Within this time period, the mean kinetic energy increases very rapidly (see Fig. 1). The updrafts start to collapse after 1.5 h integration and become organized into group structures from about 2.5 h (when the mean kinetic energy reaches a maximum). Finally, only one updraft is left as the mean kinetic energy approaches the equilibrium state.

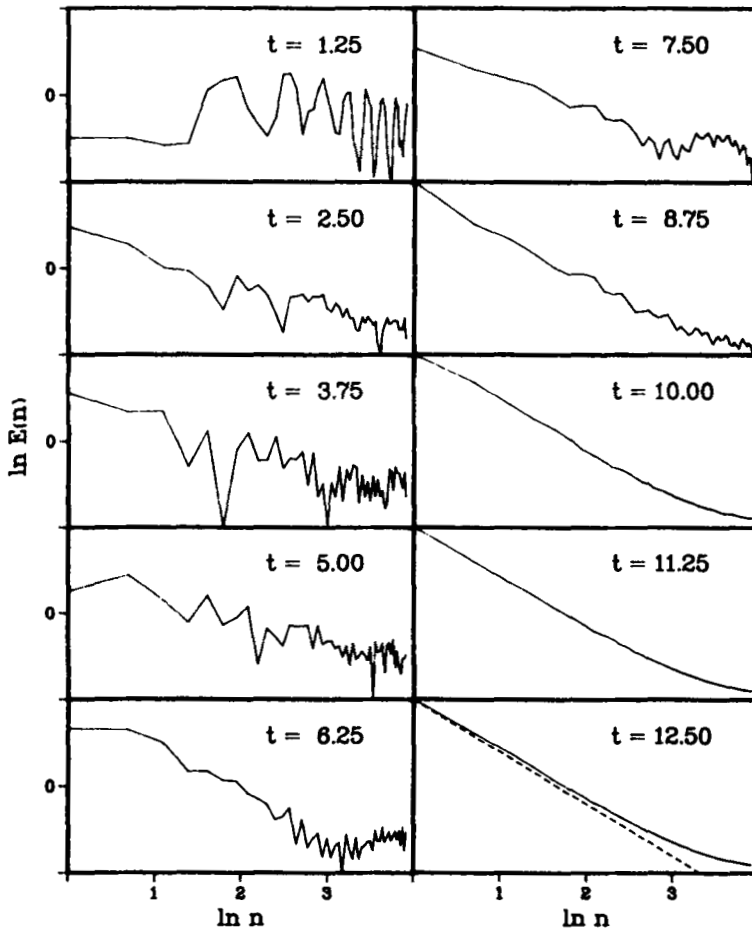


Fig. 2. Normalized kinetic energy spectrum ($E(n)$) at different time instances. Logarithmic scales are used. The dashed line is the -2 spectrum mentioned in the text. The parameters are the same as those in Fig. 1.

During the onset of convection and the final stage of the numerical simulation, each updraft covers only one grid point. This is due to the truncation scale of the model which is about 2 km. In order to obtain updrafts which cover more than one grid point, smaller scales (<300 m, with the parameters we used) need to be resolved; on these scales, the horizontal diffusion is of the same order as the buoyancy driving.

The height of the model domain has been assumed to be constant. As the spectral model is highly truncated in the vertical direction, the development of a mixed layer and its interaction with convection cannot be described. Another

limitation from the low resolution in the vertical is the absence of vorticity advection, which is very important in dry convection problems. To show the generality of the above results, we consider a grid-point model. Instead of using (2.11) with spectral truncation at $N=50$, we perform numerical integrations of (2.1) on a $N_y \times N_z$ grid for the same set of parameters used in the above computations. Here N_y and N_z are the numbers of grid points in the y - and z -directions. We choose $N_y = 100$, which is equivalent to $N=50$ in the spectral truncation, and $N_z = 9$, which gives more degrees of freedom in the grid-point model of (2.1) than in the spectral model (2.11). The Arakawa Jacobian (Arakawa,

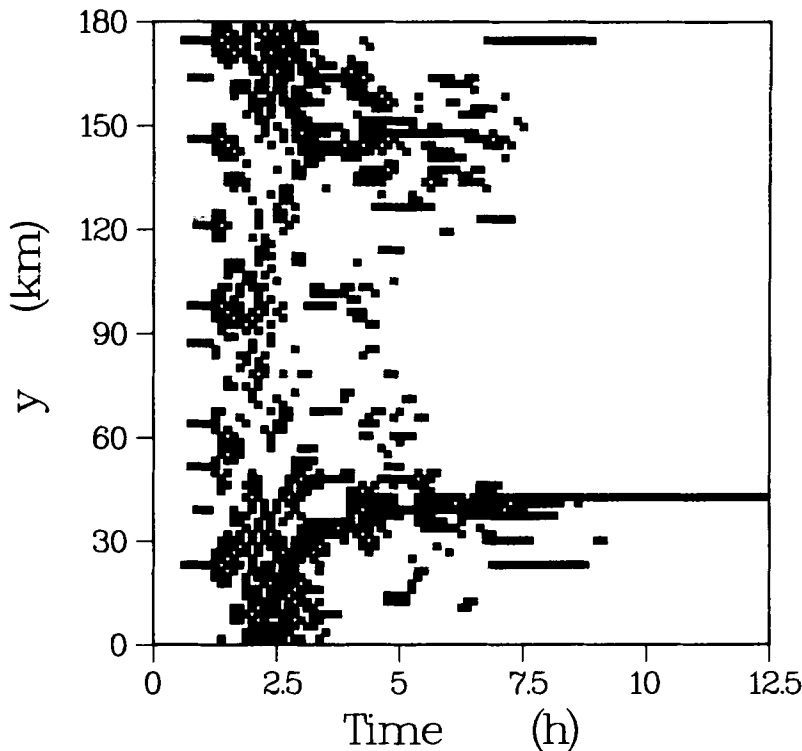


Fig. 3. The time evolution of the updraft pattern. The whole horizontal domain is shown. An updraft with its maximal vertical velocity greater than 10^{-1} m s^{-1} is denoted by a square. The parameters are the same as those in Fig. 1.

1966) is used to compute the advections of the vorticity and the temperature deviations. A staggered grid scheme is used in the space domain and a leapfrog scheme is used for time integrations, including the time filtering scheme (3.1). The streamfunction Ψ is obtained from the vorticity $\nabla^2 \Psi$ by solving the Laplace equation numerically. The time evolution of the updraft pattern up to $t = 2 \text{ h}$ is shown in Fig. 4. The upper panel, which corresponds to Fig. 3 (up to 2 h), shows the t - y cross section at the middle level $z = \frac{1}{2}d$. The agreement between the two figures is evident, which may verify that the condensational heating is dominant over the vorticity advection and the high resolution in the vertical does not alter the characteristics of the model. The lower panel of Fig. 4 shows an example of a t - z cross section and the evolution of the updraft pattern. We see that the convection cell extends from bottom to top shortly (in this case, 10 min)

after it merges. This supports the spectral truncation adopted in (2.9).

In the atmosphere, we often find situations where cold continental air is advected over warm ocean areas during winter. This is an example of the development of convection (Walter, 1980). Under certain circumstances, the convection first becomes organized into streets which are aligned in the direction of the wind and persists for several hundred kilometers. The ratio between λ , the mean horizontal distance between the clouds, and d , the height of the boundary layer, is about 6:1 before three-dimensional cellular convection takes place. The height of the boundary layer changes very little in the beginning and then grows rapidly during the transition from two-dimensional convective rolls into three-dimensional cells. Our present model is a two-dimensional model and a constant model height is assumed. If we assume the two-dimensional (y, z)

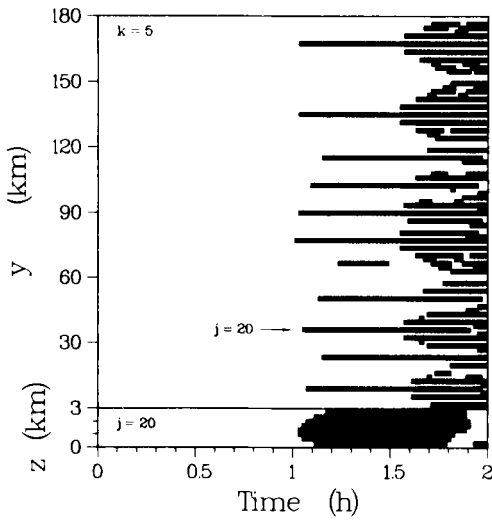


Fig. 4. The time evolution of the updraft pattern from grid point model. The upper panel shows a t - y cross section at $z = d/2$ ($k = 5$). The lower panel shows a t - z cross section at a chosen y ($j = 20$), which is indicated in the upper panel. A grid point with its vertical velocity greater than 10^{-1} m s^{-1} is denoted by a square. The parameters are the same as those in Fig. 1, but instead of $N = 50$ for spectral truncation, we have $N_x = 100$ and $N_z = 9$ for grid resolution. See the text for further explanations.

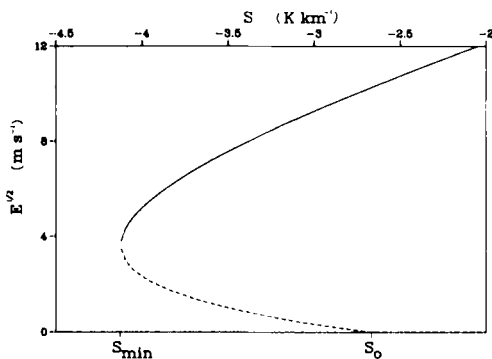


Fig. 5. Equilibrium state curves of the low-order model. The vertical axis is the square root of the equilibrium mean kinetic energy ($E^{1/2}$) and the horizontal axis is the static stability (S). The dashed lines are unstable equilibria. S_0 is the critical static stability for the onset of the convection and S_{\min} is the minimum value of S for the maintenance of the convection. The parameters are the same as those in Fig. 1, but a different aspect ratio is used: $a = 1$.

plane to be moved by a constant wind u which is perpendicular to the (y, z) plane, the model results before the initial updrafts collapse are relevant to the atmospheric situation described above. In other words, the model may be used to describe the development of convective rolls and condensational heating can be considered as one of the factors which determine the aspect ratio of the rolls observed in the atmosphere. We see from Fig. 3 and Fig. 4 that during this period, $\lambda/d = 6$ for the spectral model and $\lambda/d = 5$ for the grid-point model, which are close to that observed in the atmosphere.

4. Hysteretic behaviour of moist convection

When only one horizontal wave component in (2.11) is taken into account (Ψ_1 for the streamfunction and Θ_1 for the temperature deviation), a low-order model with a total of four components (Ψ_1 , Θ_1 , Θ_s and Θ_h) is obtained (Huang and Källén, 1986). Due to the simplicity of the low-order model, we are able to determine the model properties analytically. By examining the stability of the equilibrium states of the low-order model following a standard linear stability analysis, we find a hysteretic behaviour of moist convection, i.e., the static stability S has to be increased to S_0 , the critical static stability for onset of convection, in order to initiate convection, but once convection exists, it may be maintained even when $S < S_0$. In Fig. 5, an example is given where the mean kinetic energy E is an equilibrium state is shown as a function of the static stability. The full lines in the figure represent stable equilibrium states and S_{\min} is the minimum value of the static stability for the maintenance of convection.

The difference between S_0 and S_{\min} (ΔS) indicates the existence and significance of the hysteretic behaviour of moist convection. It has been shown in the low-order model that ΔS mainly depends on the height of the LCL and the dissipation time scale which is the time scale we used in the nondimensionalization scheme (2.6). The hysteretic behaviour exists within an atmospherically realistic range of parameter values. The most important requirement for the exist-

ence of the hysteretic behaviour is that the maximum of condensational heating should be in the lower part of the model domain. This will have a destabilizing effect on the mean stratification of the model so that convection will be further enhanced. This positive feedback between convection and the flow-dependent heating is the physical mechanism behind the hysteretic behaviour of the low-order model.

Based upon the above qualitative discussions, we now wish to investigate the hysteretic behaviour of the model by integrating the model equations (2.11) with a static stability which varies linearly in time. We have demonstrated in the previous section that when the model is unstable, it will jump from a state of no motion to a quasi-equilibrium state of convection. The growing stage is completed in about 2.5 h (1 non-dimensional unit) and an equilibrium state is obtained in around 10 h (4 non-dimensional units). To obtain the hysteretic behaviour of moist convection as a steady-state feature of the model, we vary the static stability very slowly, i.e., try to keep the model in a quasi-equilibrium state in every time step. This integration should only be viewed as a numerical way of assessing S_0 and S_{min} . In Fig. 6, we show the kinetic energy as a function of S and we believe that the model is in a quasi-equilibrium state throughout the whole time integration period except when it shows the

sudden transitions. At the beginning, the model is stable, i.e., the random forcing at each component is overcome by the dissipation term and the kinetic energy E is therefore almost zero. When S_0 is reached, a sudden jump of E indicates a loss of stability. Further increase of S gives a smooth increase of E implying that the model is in a new quasi-equilibrium state. After $t = 100$ (non-dimensional units) we reverse the process, i.e., decrease S . We see from Fig. 6 that E decreases smoothly and the convection remains even when S becomes smaller than S_0 . Finally, convection terminates after S is below S_{min} .

There are three aspects of this simulation result which we wish to discuss. Firstly, S_0 obtained here is smaller than that obtained from the low-order model. This is due to the presence of many motion scales, which enables us to resolve the flow field in such a fashion that the decelerating effect in the stable descending region is decreased significantly. The comparison between the S_0 obtained in this simulation and that in the low-order model (see Fig. 5) can be made by using the Slice Method (Bjerknes, 1938). According to Bjerknes' theory, the condition for convection to start in a conditionally unstable stratification is

$$U/D = (\Gamma - \Gamma_m)/(\Gamma_d - \Gamma), \tag{4.1}$$

where U is the area of ascending motion and D is the area of descending motion. In (4.1), the effect of dissipation is neglected. This is acceptable due to the choice of the nondimensional time scale, defined in (2.6), in all simulations discussed above. As we pointed out in the low-order model study, when the nondimensional time scale is longer than 2 h, S_0 does not depend strongly on dissipation (Huang and Källén, 1986). From (4.1) and recalling the definition of the static stability $S = \Gamma - \Gamma_d$, we get the following expression for S_0

$$S_0 = (\Gamma_m - \Gamma_d) D / (U + D). \tag{4.2}$$

In the low-order model where $U/D = 1$ and Γ_m is about 5 K km^{-1} , S_0 is indeed around -2.5 K km^{-1} (see Fig. 5). On the other hand, if we neglect the influence of downdrafts completely, S_0 will be -5 K km^{-1} . The S_0 obtained from the high resolution model is -4.25 K km^{-1} which gives $U/D = 0.18$, a number fairly close to that obtained in Fig. 5 during the onset of convection (e.g., $t = 1 \text{ h}$). Secondly, the amplitude of the mean kinetic energy in a quasi-equilibrium state

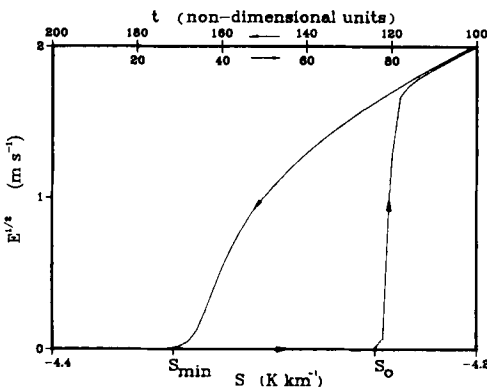


Fig. 6. Mean kinetic energy as a function of the static stability. The time scale used in numerical integration is also given in nondimensional units. The parameters are the same as those in Fig. 1.

of convection is smaller than that of the low-order model, which implies that the condensational heating used in the low-order model is overestimated. Thirdly, S_{\min} is almost unchanged. The difference between S_0 and S_{\min} in Fig. 6 is smaller than that in Fig. 5, which means that the hysteretic behaviour of the high resolution model is not as pronounced as in the low-order model.

To confirm this simulation result, we have performed another experiment where the model parameters are the same as in Fig. 6, but the process of varying the static stability is reversed, i.e., we proceed the numerical integration from a larger S to a smaller one and then increase it again. The results from this simulation (the amplitude of the mean kinetic energy, the values of S_0 and S_{\min} , etc.) are almost exactly the same as those shown in Fig. 6. A few more experiments with different random forcing series and/or different acting time periods show that the model results in the steady-state study do not depend on the random forcing terms as long as their amplitudes are sufficiently small. Parameter sensitivity studies on the hysteretic behaviour have been done numerically following the guidance of the low-order model (see Huang and Källén, 1986). Although ΔS is found to be fairly small in the above integration, it can be much larger if the model parameters are altered accordingly, for instance with a weaker dissipation. There is no doubt that the hysteretic behaviour is an intrinsic model property.

Under atmospheric conditions, convection may be considered as a transient phenomenon and it may be more interesting to investigate the transient solution of the model. We let the process of increasing static stability from a stable stratification to a conditionally unstable one and the reversed process be completed in 24 h and wish to model the diurnal cycle of the cumulus activity described in Section 1. In Fig. 7, we show the mean kinetic energy as a function of time. The time evolution of the static stability is also given. The choice of the upper and lower limits for the variation of S is a bit arbitrary. They should be within an atmospherically realistic range and include both S_0 and S_{\min} . The values of S_0 and S_{\min} indicated in Fig. 7 are determined from the steady-state study shown in Fig. 6. The hysteretic behaviour is enhanced by an inertia effect which is dependent on the time scale for

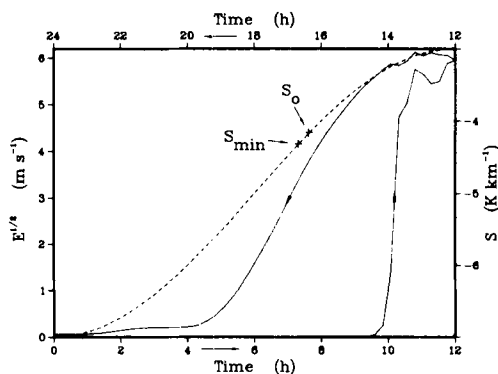


Fig. 7. Mean kinetic energy as a function of time (full line). The time evolution of the static stability (dashed line). The parameters are the same as those in Fig. 1.

changing S . Before $t = 8$ (h), the stratification is already conditionally unstable ($S > S_0$) but the jump in the mean kinetic energy E occurs after $t = 9$ (h), i.e., more than 1 h is needed for the model to deviate significantly from a state of rest. When the stratification becomes stable again ($S < S_{\min}$), no drastic change of E appears. The decrease of E proceeds even slower when E approaches zero. The energy redistribution among different scales may also play a role in enhancing hysteretic behaviour. The time evolution of the updraft pattern is shown in Fig. 8. During the time period when the stratification is conditionally unstable, the evolution of the updraft pattern shows the same features as those discussed in Section 3 (where a constant static stability is used). However, in this simulation, the stratification becomes stable again before an equilibrium state is really reached and the flow pattern with only one updraft has therefore not been completely established. After $S > S_0$, small random perturbations organize to a pattern which is then kept throughout the sudden jump in E . Around the time when S decreases to S_{\min} , E decreases with a relatively unchanged pattern, in which there is a main updraft which covers more than one grid point and has a much larger vertical velocity than other updrafts. Although the change in E after $t = 17$ (h) shows no new feature than a smooth decrease, the updraft pattern changes from a large scale to smaller scales and finally disappears.

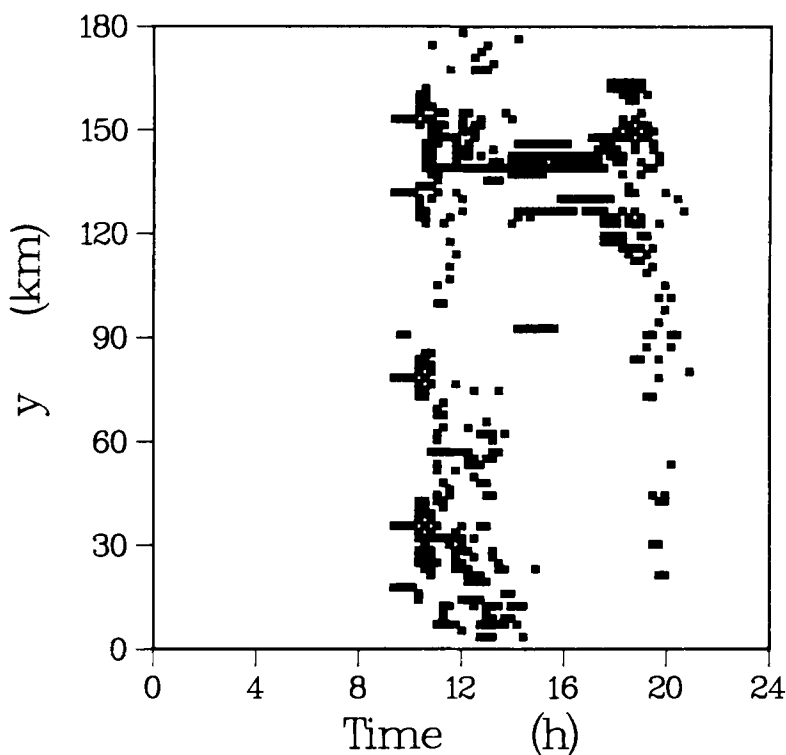


Fig. 8. The time evolution of the updraft pattern with a variable static stability shown in Fig. 7. An updraft with its maximum vertical velocity greater than 10^{-1} m s^{-1} is denoted by a square. The parameters are the same as those in Fig. 1.

5. Conclusions

We performed a study of two-dimensional moist convection with a Boussinesq-approximated model, where the effect of moisture is only taken into account as a flow-dependent heating. We extended the previous low-order model of Huang and Källén (1986) to include 100 horizontal wave components. Due to the non-linear nature of the condensational heating, the numerical method described in Section 2 has been implemented.

We first investigated the model characteristics with a constant static stability, which is conditionally unstable. Three distinct regimes are observed: (1) growing stage, in which the mean kinetic energy increases rapidly with a preferred motion pattern which appears after about 1 h; (2) grouping stage, in which the preferred motion pattern collapses and some group structures

develop; (3) final stage, in which the model approaches its equilibrium state and only one updraft is left.

By numerically integrating the high resolution model with a slowly varying static stability, we observe hysteretic behaviour as a quasi-equilibrium property of the model. The positive feedback between condensation and convection has been preserved in the high-resolution model, but the condensational heating used in the low-order model has been overestimated. The hysteretic behaviour is found to be an intrinsic property of the model.

When the time scale for changing the static stability is comparable with reality, the time evolution of the updraft pattern shows a clear difference between the onset and the termination of convection. The sudden transition from a state of rest to a quasi-equilibrium state of convection is clearly shown in the experiments and the

process is completed in about 1 h. The transition from a steady convective state to a state of no motion is slow.

Because the cumulus-scale is too small to be resolved by the resolution of large-scale models of the atmosphere, cumulus heating, moistening, cloud coverage, etc., have to be parameterized by using the model variables which represent mean values of an area of about $100 \text{ km} \times 100 \text{ km}$. Parameterization schemes are based upon observations and cumulus-scale or mesoscale model studies. The present model manifests one important effect of cumulus convection, i.e., the positive feedback between latent heat release and convection, and may therefore be seen as one of the aforementioned mesoscale models. We found a range of parameter values within which two equilibrium states are possible. Which one is realized depends on the history of moist convection and the amplitude of the perturbations. This leads to some difficulties in parameterization as the amplitude of the perturbations is unknown. Even if the perturbations are negligible, a time factor is needed in order to start or terminate moist convection, because the criterion for the onset is different from that for the termination. We have

shown that with the same set of large-scale parameters, moist convection has quite different transient characteristics in different stages of development. In particular, we found a pronounced time lag of the onset of convection after the instability has set in, a preferred convection pattern at the beginning and group structures later on. It thus seems difficult to relate subgrid scale quantities directly to large-scale variables. In order to get better detailed forecasts, a separate mesoscale model may be run with the large-scale variables as control parameters. It is impossible in the near future to consider the feedback on large-scale motion from a great number of mesoscale models in the same time unless some very simple mesoscale model can be constructed theoretically or empirically.

6. Acknowledgements

I would like to thank Dr. Erland Källén for his encouragement. He also read the manuscript and made numerous suggestions and comments. I also want to thank Professor Bert Bolin, Dr. Hans Oerlemans, Dr. Brian Reinhold and two anonymous reviewers for useful comments on this study.

REFERENCES

- Arakawa, A. 1966. Computational design for long-term numerical integrations of the equations of fluid motion: two-dimensional incompressible flow. Part I. *J. Comput. Phys.* 1, 119–143.
- Bjerknes, J. 1938. Saturated ascent of air through a dry-adiabatically descending environment. *Q. J. R. Meteorol. Soc.* 64, 325–330.
- Huang, X.-Y. and Källén, E. 1986. A low-order model for moist convection. *Tellus* 38A, 381–396.
- Krishnamurti, R. 1968. Finite amplitude convection with changing mean temperature. Part I. Theory. *J. Fluid. Mech.* 33, 445–455.
- Krishnamurti, R. 1975a. On cellular cloud patterns. Part I. Mathematical model. *J. Atmos. Sci.* 32, 1353–1363.
- Krishnamurti, R. 1975b. On cellular cloud patterns. Part 3. Applicability of mathematical and laboratory models. *J. Atmos. Sci.* 32, 1373–1383.
- Oerlemans, J. 1983. On the intensity of atmospheric convection. *Beitr. Phys. Atmos.* 56, 341–353.
- Sheu, P., Agee, E. M. and Tribbia, J. J. 1980. A numerical study of physical processes affecting convective cellular geometry. *J. Meteorol. Soc. Japan* 58, 489–499.
- Walter, B. A. 1980. Wintertime observations of roll clouds over the Bering Sea. *Mon. Wea. Rev.* 108, 2024–2031.